Radio Science®

RESEARCH ARTICLE
10.1029/2023RS007857

A Simple Noncontact Soil Moisture Probe for Weather and Climate Applications

A. G. Voronovich[1], P. E. Johnston[1,2], and R. J. Lataitis[1,3]

[1]U.S. Department Commerce/National Oceanic and Atmospheric Administration/Physical Sciences Laboratory, Boulder, CO, USA, [2]University of Colorado/Cooperative Institute for Earth System Research and Data Science, Boulder, CO, USA, [3]Science and Technology Corporation, Hampton, VA, USA

Key Points:

- Soil moisture is a critical quantity relevant for many geophysical applications
- A wide variety of techniques can be used to infer soil moisture, each with its own set of advantages and disadvantages
- A simple, noncontact method using a low-frequency antenna operating near the soil surface can be used to map bulk soil moisture

Correspondence to:

A. G. Voronovich, P. E. Johnston and R. J. Lataitis,
alexander.voronovich@noaa.gov;
paul.e.johnston@noaa.gov;
richard.lataitis@noaa.gov

Citation:

Voronovich, A. G., Johnston, P. E., & Lataitis, R. J. (2024). A simple noncontact soil moisture probe for weather and climate applications. *Radio Science*, *59*, e2023RS007857. https://doi.org/10.1029/2023RS007857

Received 23 AUG 2023
Accepted 12 AUG 2024

Author Contributions:

Conceptualization: A. G. Voronovich, P. E. Johnston, R. J. Lataitis
Formal analysis: A. G. Voronovich
Methodology: A. G. Voronovich, P. E. Johnston
Project administration: R. J. Lataitis
Writing – original draft: A. G. Voronovich
Writing – review & editing: P. E. Johnston, R. J. Lataitis

Abstract The measurement of soil moisture is important for many practical applications. We describe the theoretical design of a simple, noncontact, electromagnetic probe that complements many existing soil moisture measurement techniques. The approach uses a low-frequency (i.e., 50–150 MHz) antenna operating in proximity of the soil. The presence of the soil affects the antenna input impedance, which in turn depends on the distance between the soil and antenna and the complex dielectric constant of the soil. The latter strongly depends on the soil wetness, which suggests that bulk soil moisture integrated over a depth of roughly 1 m can be inferred from antenna impedance measurements. This is in contrast with many current higher-frequency techniques that penetrate only a few centimeters into the soil and provide only near-surface values of soil wetness. Our work suggests that under ideal conditions bulk soil moisture can be mapped with an accuracy on the order of 1% over horizontal scales spanning a few tens of meters to a few kilometers using simple low-frequency antennas.

Plain Language Summary Soil moisture information to depths of 1 m is critical for a variety of geophysical applications, including the accurate forecasting of precipitation, river flow levels and floods, and drought prediction and monitoring. While there are a large number of remote sensing techniques available that measure surface moisture values, relatively few if any can access deeper so-called root-zone depths. We present theoretical results for a noncontact technique that uses a simple, thin-wire, loop antenna operating at 50–150 MHz and a height of approximately 1 m above the soil surface to infer bulk soil moisture properties integrated over a depth of roughly 1 m with an accuracy on the order of 1% under ideal conditions. In principle, the technique can be applied using a moving vehicle or drone to map soil moisture over horizontal length scales that bridge the gap between in-situ measurements and regional-scale satellite retrievals.

1. Introduction

The measurement of soil moisture (SM) is important for many practical applications. It is a key hydrologic state variable that links land surface and atmospheric processes. Its spatial and temporal distribution has a profound impact on agricultural health, drought and flood forecasting, forest fire prediction, water supply management, and climate variability and change (Babaeian et al., 2019; Robock, 2003; Seneviratne et al., 2010). The accurate measurement of soil moisture is critical for the understanding, modeling, and prediction of associated hydrologic and atmospheric processes that are used to inform a wide range of government agencies and private companies concerned with weather forecasting and climate prediction, drought mitigation, runoff potential and flood control, soil erosion and slope failure, and reservoir management (https://weather.ndc.nasa.gov/landprocess/).

There is a wide array of SM measurement techniques spanning many decades of development. Each approach has its advantages and limitations. Recent reviews that summarize the state-of-the-art can be found throughout the literature (e.g., Babaeian et al., 2019; Hardie, 2020; Li et al., 2021; Mukhlisin et al., 2021; Susha Lekshmi et al., 2014). For the purposes of comparison, it is convenient to group the various approaches into remote (satellite and airborne), proximal (near-ground, noncontact), and ground-based (in-ground, in situ) categories (Babaeian et al., 2019), with the remote and ground-based systems offering broad-areal and continuous single-station coverage, respectively, and proximal systems offering the possibility of greater ease of application and incorporation of mobile techniques allowing for mapping of SM over horizontal scales on the order 10–1,000 m bridging the gap between point and regional coverage.

Electromagnetic (EM) approaches span all three categories. A comprehensive review can be found in Babaeian et al. (2019), with a more focused discussion of remote, proximal and ground-based methods presented by Li

et al. (2021), Hardie (2020), and Mukhlisin et al. (2021), respectively. In particular, Babaeian et al. (2019) describe a number of proximal EM induction approaches (e.g., see Section 4.2) with a focus on noncontact methods (e.g., see Figure 4). A more limited review of remote and proximal EM techniques is provided by Voronovich and Lataitis (2021, 2022).

In this work we consider one proximal EM technique in detail: that of a horizontally-oriented antenna operating in the near field above the surface of the soil. The presence of the soil affects the input impedance of the antenna, which depends on the distance between the soil and the antenna and the complex dielectric constant of the soil, the latter in turn depending strongly on soil wetness. The theoretical basis for this approach was considered in a number of earlier studies (e.g., Chang, 1973; Kennedy, 1956; Ryu et al., 1970; Spears, 1989; Wait & Spies, 1972), but the technique as a remote probing tool was not actively pursued at the time, possibly due to insufficient capabilities of earlier-day electronics.

We revisit this concept and use numerical simulations to assess its potential as a practical soil moisture measurement technique. The simulations are based on a theoretical approach that was developed recently for the calculation of bent, thin-wire antennas operating in free space (Voronovich et al., 2023). We extend this theory to account for the interaction between a thin-wire, loop antenna and a vertically stratified, dielectric half-space. The resulting equation for the input impedance of the antenna (or, equivalently, for its resonant frequency) as a function of the complex dielectric constant is applicable to loop antennas of any shape and can, in particular, be expressed in closed form for a circular loop antenna. We note that in contrast with earlier work our general result has no restriction on the type of antenna that can be used for this measurement nor on the proximity of the antenna to the soil surface. We consider a circular loop antenna only because it yields a relatively straightforward and easily-computable closed-form solution that allows us to illustrate the main points of this work. Our result is applicable in both the near- and far-field of the antenna.

Using this result we demonstrate numerically that a low-frequency (i.e., 50–150 MHz) circular loop antenna of about a meter in diameter, horizontally oriented at a height of the same order above the soil surface, can be used to retrieve bulk-averaged soil moisture to a good accuracy. We suggest a simple idealized circuit comprising a variable capacitor and loop antenna driven by a narrowband signal to illustrate in principle how this measurement could be implemented.

The primary novelty of our approach over existing techniques is that the use of lower frequencies allows for deeper probing into the soil and a more representative bulk soil wetness measurement, and that its portable, noncontact nature permits mounting on surface vehicles or drones that can provide soil moisture measurements over horizontal scales that bridge the gap between in-situ measurements and regional satellite retrievals. These intermediate scales are typically inaccessible using many current technologies but are important for informing many natural resource management decisions (e.g., as related to extreme precipitation and flooding, droughts and associated crop failure and famine, general agricultural health, water resource and dam management, wildfire prediction and mitigation, and ecosystem health) in addition to allowing for more accurate representations of soil moisture variability in numerical models leading to improved extreme precipitation and flood forecasts and drought projections. Finally, this is a relatively simple technique that is straightforward and inexpensive to implement compared to, for example, manned aircraft measurements that might sample similar intermediate scales.

2. Loop Antenna in Free Space

This section briefly summarizes an earlier theoretical development by Voronovich et al. (2023) for the current j_s in a thin-wire, loop antenna operating in free space. Equation 1 expresses the current in terms of its Fourier harmonics $\hat{j}_n$, and Equation 2 below relates the amplitudes of the Fourier harmonics to the electric field incident on the antenna. These equations together with the supporting expressions (Equations 3–7) are used to evaluate the complex antenna input impedance described in Sections 3–5.

We express the electric current j_s excited in a thin-wire, loop antenna by an incident electric field $\vec{E}_{in}$ with angular frequency $\omega = 2\pi$ in free space in terms of its harmonics $\hat{j}_n$ as:

$$j_s = \sum_{n=-\infty}^{\infty} \hat{j}_n \exp\left(2\pi i n \frac{s}{L}\right), \tag{1}$$

where the governing equation for $\hat{j}_n$ is given by (see Equation 32 in Voronovich et al., 2023):

$$\left(i\pi\frac{c^2}{\omega^2}K_n^2H_0^{(1)}(K_na)J_0(K_na)+v_n\right)\hat{j}_n+\sum_{m=-\infty}^{\infty}V_{nm}\hat{j}_m=i\frac{4\pi\varepsilon_0c^2}{\omega L}\int_{-L/2}^{L/2}e^{-2\pi ins/L}\vec{E}_{in}\left(\vec{R}_s\right)\cdot\frac{d\vec{R}_s}{ds}ds. \quad (2)$$

Here L is the total wire length, a is the radius of the wire, s is the arc length along the wire $(-L/2<s<L/2)$, $\vec{R}_s$ is a 3D vector at a point on the wire along the arc length s,

$$K_n=\left(\frac{\omega^2}{c^2}-\left(\frac{2\pi}{L}n\right)^2\right)^{1/2},\ \ \mathrm{Im}K_n\geq 0, \quad (3)$$

and

$$v_n=4(-1)^n\frac{i\omega L/c-2}{(\omega L/c)^2}\exp\left(i\frac{\omega L}{2c}\right)-\frac{c^2}{\omega^2}K_n^2\left[Ei\left(i\frac{\omega L}{2c}+i\pi n\right)-Ei\left(i\frac{\omega L}{2c}-i\pi n\right)\right], \quad (4)$$

where

$$Ei(ix)=\int_1^{\infty}\frac{e^{ixt}}{t}dt \quad (5)$$

is an exponential integral function of imaginary argument. The dimensionless interaction matrix V_{nm} doesn't depend on the wire radius a and is given by the following integral:

$$V_{nm}=\frac{\omega}{cL}\int_{-L/2}^{L/2}\int_{-L/2}^{L/2}V\left(s,s'\right)\exp\left(-i\frac{2\pi}{L}\left(ns-ms'\right)\right)dsds', \quad (6)$$

where

$$\begin{aligned}\frac{\omega^3}{c^3}V\left(s,\,s'\right)=&\left(-\frac{2}{|s-s'|^3}+\frac{2i\omega/c}{(s-s')^2}\right)\exp\left(i\frac{\omega}{c}|s-s'|\right)+\frac{\exp(i\omega\rho/c)}{\rho^3}\left[\left(\frac{\omega^2\rho^2}{c^2}+i\frac{\omega\rho}{c}-1\right)\right.\\&\left.\times\left(\frac{d\vec{R}_s}{ds}\cdot\frac{d\vec{R}_{s'}}{ds'}\right)-\left(\frac{\omega^2\rho^2}{c^2}+3i\frac{\omega\rho}{c}-3\right)\left(\frac{\vec{R}_s-\vec{R}_{s'}}{\rho}\cdot\frac{d\vec{R}_s}{ds}\right)\left(\frac{\vec{R}_s-\vec{R}_{s'}}{\rho}\cdot\frac{d\vec{R}_{s'}}{ds'}\right)\right]_{\rho=\left|\vec{R}_s-\vec{R}_{s'}\right|}.\end{aligned} \quad (7)$$

It is important to note that the singularities that appear within the first parenthesis on the right-hand side (RHS) of (7) cancel and the function $V(s,s')$ is in fact non-singular. For the case of a circular loop antenna the matrix V_{nm} becomes diagonal and $V(s,s')$ can be expressed in closed form and the corresponding input admittance calculated numerically.

Figure 1 describes the input admittance of a thin-wire, circular loop antenna as a function of loop diameter. It is copied from an earlier work examining the electrical characteristics of thin-wire antennas (Voronovich et al., 2023). It is consistent with the development presented here and illustrates the favorable agreement between the theoretical expressions for the real and imaginary parts of the input admittance for a circular loop antenna with a δ-gap excitation and the corresponding experimental data presented by Kennedy (1956).

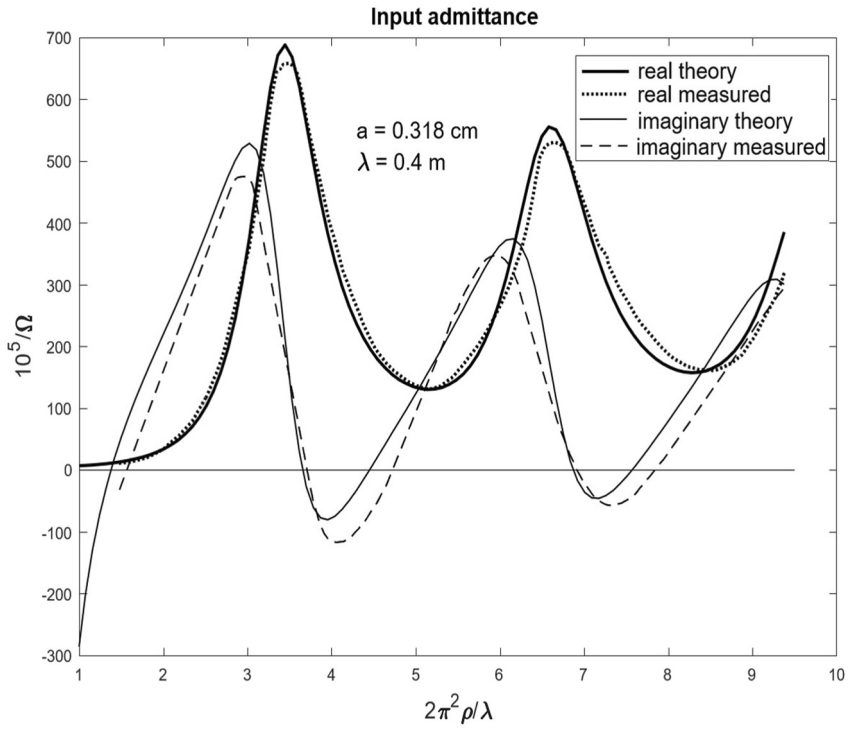

Figure 1. The theoretical input admittance of a thin-wire, circular loop antenna with a δ-gap excitation as a function of the normalized loop diameter $2\rho\pi^2/\lambda$, where ρ is the antenna radius, a is the wire radius, and λ is the free space wavelength. Both the real and imaginary parts of the admittance (solid and dashed lines, respectively) are shown (Figure 5 from Voronovich et al., 2023. Measured data from Kennedy, 1956).

3. Loop Antenna Over a Vertically Stratified Half-Space

Now let us consider a loop antenna operating over a vertically stratified half-space. The typical way to feed the antenna is to apply a voltage at a certain point; in this case the incident field $\vec{E}_{in}$ in the RHS of Equation 2 becomes a delta-function. In this section we consider the general case of an arbitrary $\vec{E}_{in}$. We also consider the case of a loop antenna of arbitrary shape. We assume the properties of the half-space depend only on vertical coordinate z with the z-axis directed upward, and that its upper boundary is a horizontal plane. Since the EM field radiated by the loop antenna is partially reflected by the half-space, the incident electric field $\vec{E}_{in}$ in the RHS of Equation 2 is modified. The corresponding modification to Equation 2 is considered in detail in this section.

First we calculate the electric field generated by an arbitrary distributed current in the loop antenna, which is represented as a sum of its Fourier harmonics. The calculation proceeds in the Fourier domain, and the resulting field is expressed as a superposition of plane waves of vertical and horizontal polarization (Equation 16 below). Each plane wave is reflected from the stratified medium below the antenna with a known reflection coefficient. (The calculation of the reflection coefficient from a vertically stratified medium is a separate task and is described in Voronovich and Lataitis (2021) and elsewhere). Using the superposition principle, we obtain as a result an expression for the field reflected from the soil in terms of the Fourier harmonics of the current in the antenna. This field has to be added to the original excitation field $\vec{E}_{in}$ in the RHS of Equation 2. As a final result we obtain Equation 27 as the governing expression for the current in a loop antenna operating over a stratified medium in terms of is Fourie harmonics. We emphasize that the loop antenna can be of arbitrary shape and arbitrarily close to the soil as no far-field approximation was used in the development.

The general equation for the electric field $\vec{E}$ generated by a spatially distributed current with density $\vec{j}$ can be expressed as (e.g., Jackson, 1999):

$$\left(\frac{\omega^2}{c^2}+\nabla^2\right)\vec{E}=-\frac{i}{\varepsilon_0\omega}\left(\frac{\omega^2}{c^2}\vec{j}+\nabla\left(\nabla\vec{j}\right)\right). \tag{8}$$

Let us represent $\vec{E}$ and $\vec{j}$ in terms of their 3D Fourier transforms:

$$\vec{E}_{\vec{R}}=\int \vec{E}_{\vec{K}}e^{i\vec{K}\cdot\vec{R}}d\vec{K}, \tag{9}$$

$$\vec{j}_{\vec{R}}=\int \vec{j}_{\vec{K}}e^{i\vec{K}\cdot\vec{R}}d\vec{K}, \tag{10}$$

where $\vec{K}$ is a 3D wave vector. In terms of these Fourier transforms Equation 8 becomes:

$$\vec{E}_{\vec{K}}=-\frac{i}{\varepsilon_0\omega}\,\frac{\omega^2/c^2\vec{j}_{\vec{K}}-\vec{K}\left(\vec{K}\cdot\vec{j}_{\vec{K}}\right)}{\omega^2/c^2-K^2+i\delta}. \tag{11}$$

We added into the denominator in Equation 11 a small attenuation term $i\delta$ ($\delta>0$), which shifts the poles from the real axes to ensure fulfillment of the limiting absorption principle, that is, after performing the corresponding integrations one sets $\delta\to+0$ so that the result in fact doesn't depend on δ.

In what follows it will be convenient to split the wave vector into its horizontal and vertical projections, that is, $\vec{K}=\vec{k}+k_z\vec{e}_z$, and similarly split the 3D coordinate vector $\vec{R}=\vec{r}+z\vec{e}_z$ into its transverse and longitudinal directions. Let us introduce the unit polarization vectors $\vec{p}^{(1)}_{\vec{k},k_z}$, $\vec{p}^{(2)}_{\vec{k}}$ for waves of vertical and horizontal polarization, respectively:

$$\vec{p}^{(2)}_{\vec{k}}=-\frac{\vec{e}_z\times\vec{k}}{k} \tag{12}$$

and

$$\vec{p}^{(1)}_{\vec{k},k_z}=-\frac{c}{\omega}\vec{K}\times\vec{p}^{(2)}_{\vec{k}}=\frac{c}{\omega}\left(\vec{k}+k_z\vec{e}_z\right)\times\frac{\vec{e}_z\times\vec{k}}{k}=\frac{c}{\omega}\frac{1}{k}\left(k^2\vec{e}_z-k_z\vec{k}\right), \tag{13}$$

where $k=|\vec{k}|$. Note, that $\vec{p}^{(2)}_{\vec{k}}$ doesn't depend on k_z (in contrast to $\vec{p}^{(1)}_{\vec{k},k_z}$). It is clear from Equation 11 that $\vec{K}\cdot\vec{E}_{\vec{k}}=0$ (i.e., the longitudinal component of the electric field is absent, as it should be). Hence, Equation 11 can be represented as follows:

$$\vec{E}_{\vec{k}}=-\frac{i\omega}{\varepsilon_0c^2}\,\frac{\left(\vec{j}_{\vec{k},k_z}\cdot\vec{p}^{(1)}_{\vec{k},k_z}\right)\vec{p}^{(1)}_{\vec{k},k_z}+\left(\vec{j}_{\vec{k},k_z}\cdot\vec{p}^{(2)}_{\vec{k},k_z}\right)\vec{p}^{(2)}_{\vec{k},k_z}}{\frac{\omega^2}{c^2}-K^2+i\delta}. \tag{14}$$

Now we substitute Equation 14 into Equation 9. Assuming $z<0$, we can calculate the electric field below the loop by integrating over k_z using a residue at $k_z=-q_k$, where

$$q_k=\left(\omega^2/c^2-k^2\right)^{1/2},\ \mathrm{Im}\,q_k\geq 0. \tag{15}$$

One then obtains:

$$\vec{E}_{in}\left(\vec{r},z\right)=-\frac{\pi\omega}{\varepsilon_0 c^2}\int\left[\left(\vec{j}_{\vec{k},-q_k}\cdot\vec{p}^{(1)}_{\vec{k},-q_k}\right)\vec{p}^{(1)}_{\vec{k},-q_k}+\left(\vec{j}_{\vec{k},-q_k}\cdot\vec{p}^{(2)}_{\vec{k}}\right)\vec{p}^{(2)}_{\vec{k}}\right]e^{i\vec{k}\cdot\vec{r}-iq_k z}\frac{d\vec{k}}{q_k}. \quad (16)$$

Equation 16 represents an expansion of the electric field radiated by the current in the loop downward into a superposition of plane waves of vertical and horizontal polarization. Let us assume that the boundary of the half-space is located at a level $z=-h, h>0$. When propagating downwards to the boundary of the half-space and back, the waves of both polarizations acquire a phase factor $exp\ (2iq_k h)$. Due to reflection the amplitude of each plane wave has to be multiplied also by the corresponding reflection coefficient $V_k^{(1)}$ or $V_k^{(2)}$, where the upper index stands for vertical (1) or horizontal (2) polarization, and each plane wave has to change the sign of vertical component of the wave vector. As a result, the electric field of the reflected waves becomes:

$$\vec{E}_{ref}\left(\vec{r},z\right)=-\frac{\pi\omega}{\varepsilon_0 c^2}\int\left[\left(\vec{j}_{\vec{k},-q_k}\cdot\vec{p}^{(1)}_{\vec{k},-q_k}\right)V_k^{(1)}\vec{p}^{(1)}_{\vec{k},q_k}+\left(\vec{j}_{\vec{k},-q_k}\cdot\vec{p}^{(2)}_{\vec{k}}\right)V_k^{(2)}\vec{p}^{(2)}_{\vec{k}}\right]e^{2iq_k h}e^{i\vec{k}\cdot\vec{r}+iq_k z}\frac{d\vec{k}}{q_k}. \quad (17)$$

This electric field should be added to $\vec{E}_{in}$ in Equation 2, which results in the following additional term in the RHS of Equation 2:

$$\begin{aligned}I_n=i\frac{4\pi\varepsilon_0 c^2}{\omega L}\int_{-L/2}^{L/2}e^{-2\pi ins/L}\vec{E}_{ref}\left(\vec{R}_s\right)\cdot\frac{d\vec{R}_s}{ds}ds=-i\frac{4\pi^2}{L}\int_{-L/2}^{L/2}ds\int\frac{d\vec{k}}{q_k}\\ \times\left[\left(\vec{j}_{\vec{k},-q_k}\cdot\vec{p}^{(1)}_{\vec{k},-q_k}\right)\left(\vec{p}^{(1)}_{\vec{k},q_k}\cdot\frac{d\vec{R}_s}{ds}\right)V_k^{(1)}\right.\\ \left.+\left(\vec{j}_{\vec{k},-q_k}\cdot\vec{p}^{(2)}_{\vec{k}}\right)\left(\vec{p}^{(2)}_{\vec{k}}\cdot\frac{d\vec{R}_s}{ds}\right)V_k^{(2)}\right]e^{2iq_k h+i\vec{k}\cdot\vec{r}_s+iq_k z_s}e^{-2\pi ins/L}.\end{aligned} \quad (18)$$

From Equation 10 one finds:

$$\vec{j}_{\vec{k},-q_k}=\frac{1}{(2\pi)^3}\int\vec{j}_{\vec{R}}e^{-i\vec{k}\cdot\vec{r}+iq_k z}d\vec{R} \quad (19)$$

Integrating over the cross-section of the thin wire one obtains the total current in the wire at a point s multiplied by the unit vector directed along the wire axis at this point $d\vec{R}_s/ds$. The remaining integration becomes an integration over s and one finds:

$$\vec{j}_{\vec{k},-q_k}=\frac{1}{(2\pi)^3}\int_{-L/2}^{L/2}j_s e^{-i\vec{k}\cdot\vec{r}_s+iq_k z_s}\frac{d\vec{R}}{ds}ds. \quad (20)$$

Substituting into Equation 20 j_s from Equation 1 yields:

$$\vec{j}_{\vec{k},-q_k}=\frac{1}{(2\pi)^3}\sum_{m=-\infty}^{\infty}\hat{j}_m\int_{-L/2}^{L/2}e^{2\pi ims/L-i\vec{k}\cdot\vec{r}_s+iq_k z_s}\frac{d\vec{R}}{ds}ds. \quad (21)$$

Substituting Equation 21 into Equation 18 one obtains:

$$I_n=-i\sum_{m=-\infty}^{\infty}R_{nm}\hat{j}_m, \quad (22)$$

where

$$R_{nm} = \frac{1}{2\pi L}\int \frac{d\vec{k}}{q_k} e^{2iq_k h}\int_{-L/2}^{L/2} ds e^{-2\pi i n s/L + i\vec{k}\cdot\vec{r}_s + iq_k z_s}\int_{-L/2}^{L/2} ds' e^{2\pi i m s'/L - i\vec{k}\cdot\vec{r}_{s'} + iq_k z_{s'}}$$
$$\times\left[\left(\frac{d\vec{R}_{s'}}{ds'}\cdot\vec{p}^{(1)}_{\vec{k},-q_k}\right)\left(\vec{p}^{(1)}_{\vec{k},q_k}\cdot\frac{d\vec{R}_s}{ds}\right)V_k^{(1)} + \left(\frac{d\vec{R}_{s'}}{ds'}\cdot\vec{p}^{(2)}_{\vec{k}}\right)\left(\vec{p}^{(2)}_{\vec{k}}\cdot\frac{d\vec{R}_s}{ds}\right)V_k^{(2)}\right]. \quad (23)$$

We can simplify the expression for the matrix R_{nm} in Equation 23 as follows. Note that $p^{(1)}_{-\vec{k}} = p^{(1)}_{\vec{k}}$ and $p^{(2)}_{-\vec{k}} = -p^{(2)}_{\vec{k}}$. Introducing the following expressions:

$$A^{(n)}_{\vec{k}} = \int_{-L/2}^{L/2} e^{-2\pi i n s/L + i\vec{k}\cdot\vec{r}_s + iq_k z_s}\left(\frac{d\vec{r}_s}{ds} + \frac{dz_s}{ds}\vec{e}_z\right)\cdot\vec{p}^{(1)}_{\vec{k},q_k} ds, \quad (24)$$

$$B^{(n)}_{\vec{k}} = \int_{-L/2}^{L/2} e^{2\pi i n s/L - i\vec{k}\cdot\vec{r}_s + iq_k z_s}\left(\frac{d\vec{r}_s}{ds} + \frac{dz_s}{ds}\vec{e}_z\right)\cdot\vec{p}^{(2)}_{\vec{k}} ds, \quad (25)$$

one finds:

$$R_{nm} = \frac{1}{2\pi L}\int \frac{d\vec{k}}{q_k} e^{2iq_k h}\left(A^{(n)}_{\vec{k}} A^{(-m)}_{-\vec{k}} V_k^{(1)} - B^{(n)}_{\vec{k}} B^{(-m)}_{-\vec{k}} V_k^{(2)}\right). \quad (26)$$

Adding Equation 22 to the RHS of Equation 2 one obtains the following equation, which describes the behavior of a the loop antenna located over a horizontally stratified half-space:

$$\left(i\pi\frac{c^2}{\omega^2}K_n^2 H_0^{(1)}(K_n a)J_0(K_n a) + v_n\right)\hat{j}_n + \sum_{m=-\infty}^{\infty}(V_{nm} + iR_{nm})\hat{j}_m$$
$$= i\frac{4\pi\varepsilon_0 c^2}{\omega L}\int_{-L/2}^{L/2} e^{-2\pi i n s/L}\vec{E}_{in}\left(\vec{R}_s\right)\cdot\frac{d\vec{R}_s}{ds} ds. \quad (27)$$

The only difference compared to the free space result in Equation 2 is the additional term iR_{nm} in the summation over m. Note that the Fourier amplitudes of the current are complex. For a delta-excitation of the antenna the current at the point of excitation (which is given by the sum of all Fourier harmonics at that point) will also be complex, and the ratio of the feeding voltage to the total current yields the both real- and imaginary part of the impedance.

We emphasize that the interaction between a plane wave and a vertically stratified half-space is completely characterized by the corresponding reflection coefficients, and Equation 23 applies to any such half-space. For the case of a homogeneous half-space $V_k^{(1,2)}$ become the Fresnel reflection coefficients.

4. The Case of a Circular Loop Antenna

Let us assume that the loop is circular with radius r_0 located horizontally at the level $z = 0$. Setting

$$\frac{\vec{k}}{k} = \cos\theta\vec{e}_x + \sin\theta\vec{e}_y \quad (28)$$

and introducing polar angle $\varphi = s/r_0$ one finds:

$$\frac{d\vec{r}_s}{ds} = -\sin\varphi\vec{e}_x + \cos\varphi\vec{e}_y. \quad (29)$$

Simple calculations give:

$$A^{(n)}_{\overrightarrow{k}} = -\pi \frac{c}{\omega} r_0 q_k e^{-in\theta + i\pi n/2} [J_{n-1}(kr_0) + J_{n+1}(kr_0)], \tag{30}$$

$$B^{(n)}_{\overrightarrow{k}} = i\pi r_0 e^{in\theta - i\pi n/2} [J_{n-1}(kr_0) - J_{n+1}(kr_0)], \tag{31}$$

where J_n is the Bessel function. The substitution $\overrightarrow{k} \to -\overrightarrow{k}$ is equivalent to the replacement $\theta \to \theta + \pi$, and one also has $J_{-n}(z) = (-1)^n J_n(z)$. Taking this into account one notes that the products $A^{(n)}_{\overrightarrow{k}} A^{(-m)}_{-\overrightarrow{k}}$ and $B^{(n)}_{\overrightarrow{k}} B^{(-m)}_{-\overrightarrow{k}}$ are both proportional to $exp\,[i(n-m)\theta]$. For this reason, the integration in (26) over $d\overrightarrow{k} = kdkd\theta$ with respect polar angle θ yields $2\pi\delta_{nm}$. As a result one obtains:

$$R_{nm} = \delta_{nm} R_n, \tag{32}$$

where

$$R_n = \frac{\pi}{2} r_0 \int_0^\infty \frac{kdk}{q_k} e^{2iq_k h} \left(\left(-\frac{c^2}{\omega^2} \right) q_k^2 [J_{n-1}(kr_0) + J_{n+1}(kr_0)]^2 V_k^{(1)} + [J_{n-1}(kr_0) - J_{n+1}(kr_0)]^2 V_k^{(2)} \right). \tag{33}$$

The matrix V_{nm} for a circular loop is also diagonal (Voronovich et al., 2023), and the solution of the equation set in Equation 27 in this case reduces to a straightforward calculation.

5. A Soil Moisture Probe

In Figure 2 we show the dependence of the real and imaginary parts of the input impedance Z of a circular loop antenna as a function of frequency. The dielectric constant of the soil ε was calculated using the Mironov et al. (2020) model for a dry soil density of 1.575 g/cm^3 and a 9.1% clay fraction at a temperature of 20^o Celsius. The volumetric soil moisture was set to $m_v = 0.2$ g/cm^3 (corresponding to a soil saturation level of 20%) yielding a dielectric constant $\varepsilon = 11.2 + 2.1i$. One can see that at frequencies exceeding 100 MHz the difference between the free-space and dielectric half-space impedance is generally quite noticeable. The question arises if this difference can be used to measure soil moisture. Based on the theory developed in the previous section we will estimate below the feasibility of the corresponding measurements.

An idealized circuit diagram for a potential SM probe is shown in Figure 3. It is based on a simple, series, LC resonant circuit. The loop antenna constitutes the purely inductive load L. The circuit is at resonance when the corresponding reactances $X_L = 2\pi fL$ and $X_C = 1/2\pi fC$ are equal. Solving for C the resonant condition can be expressed as $C = 1/2\pi f X_L$. We assume that a continuous signal at a fixed frequency f_0 passes through a narrowband filter and feeds the loop antenna. The antenna's input reactance is purely inductive and given by Im $(Z(f_0))$.

Therefore, when

$$C = \frac{1}{2\pi f_0 \mathrm{Im}[Z(f_0)]} \tag{34}$$

the compensation is complete and the current in the circuit will be a maximum (i.e., the circuit will be at resonance). At a fixed elevation of the antenna the input impedance Z, and therefore the resonant capacitance C, are functions of the dielectric constant of soil, which depends on SM. Thus, by scanning the capacitance to find its resonant value and moving the antenna along the soil surface at a given height one can essentially map variations of the bulk SM.

Figure 4 depicts the real and imaginary parts of the input impedance and the corresponding resonant capacitance C as a function of the volumetric soil moisture m_v (in g/cm^3) for an excitation frequency $f_0 = 115$ MHz. The parameter

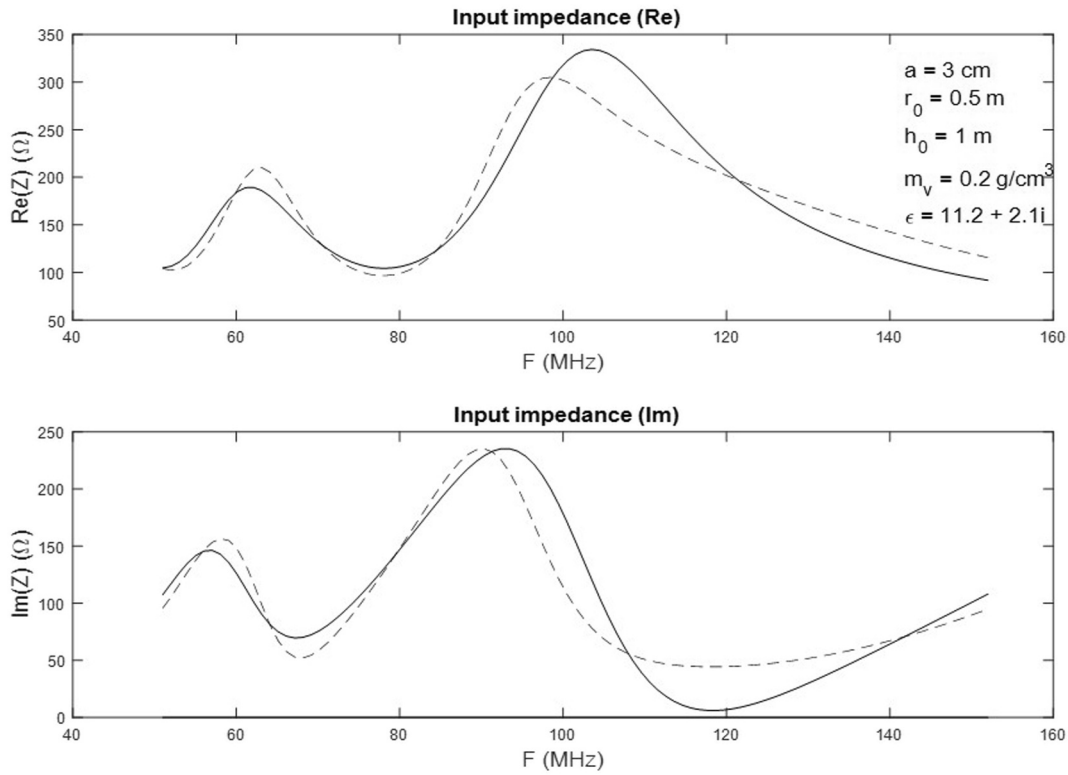

Figure 2. The theoretical dependence of the real (top) and imaginary (bottom) parts of the input impedance Z on frequency F for a circular loop antenna of radius $r_0 = 0.5$ m and wire radius $a = 3$ cm located $h_0 = 1$ m above the soil surface. The solid line describes the free space impedance and the dashed line the impedance in the presence of the dielectric half-space.

Z_0 is the loop's impedance in the free space. One can see that the dependence of C on m_v is strong for relatively low values of SM but tends to weaken for wetter soils, which suggests that the measurement sensitivity dC/dm_v decreases for wetter soils. As a lower bound on the measurement sensitivity we note that for extremely wet soils (i.e., $m_v \approx 0.4$ g/cm^3 and greater) $dC/dm_v \approx 20$ pF/(1 gm/cm^3), which should be readily detectable (e.g., see Ashrafi & Golnabi, 1999). The reduction of sensitivity for large m_v is most likely due to a significant increase in dielectric constant, which makes the soil surface behave as a perfect reflector. One can mitigate the decrease in measurement sensitivity for higher soil wetness using a multi-turn loop antenna.

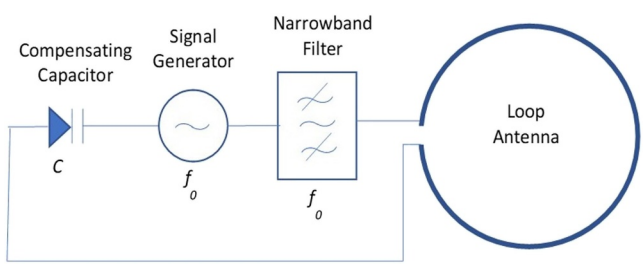

Figure 3. Idealized circuit diagram for a noncontact soil moisture probe comprising a circular loop antenna excited by a filtered continuous wave signal of frequency f_0 coupled to a compensating capacitor of capacitance C.

6. Discussion

In principle, this technique can be applied using a moving vehicle or low-flying drone to map soil moisture over scales not accessible to satellite measurements nor to more local in-situ contact probes. There are a few potential areas of concern regarding the practical application of this technique. First, there is a need to adequately control the elevation of the antenna. This can be accomplished using an ultrasonic sensor. For acoustic frequencies in the range of 20–30 KHz scattering from vegetation compared to surface reflection should be relatively weak, and measuring elevation with centimeter accuracy should be attainable. Second, there is a need to have a very stable signal generator. A quartz-based device should provide the required frequency stability. Third, the compensating capacitance needs to be measured with sufficient accuracy. There are a number technologies that can be applied that should provide the needed accuracy and precision. As examples, we refer interested readers to recent work by Moayyed et al. (2021) and Shirkolaei and Aslinezhad (2020).

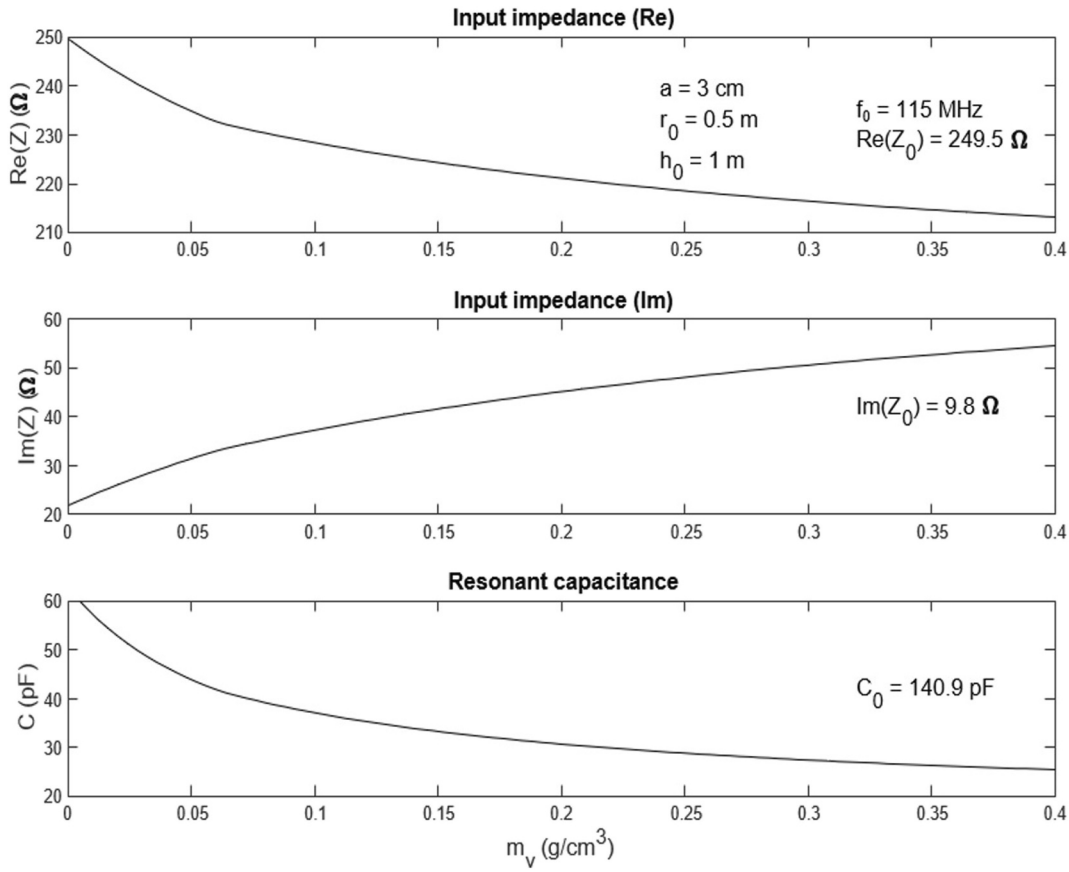

Figure 4. The theoretical dependence of the real (top) and imaginary (center) parts of the input impedance Z, and the corresponding resonant capacitance C (bottom), on volumetric soil moisture m_v for a circular loop antenna of radius $r_0 = 0.5$ m with wire radius $a = 3$ cm located $h_0 = 1$ m above the soil surface. The excitation frequency $f_0 = 115$ MHz.

7. Conclusions

We have extended an earlier theoretical development for the current in an arbitrary thin-wire loop antenna operating in free space to include a dielectric half-space. We have considered the case of a circular loop antenna in detail and noted the measurable difference between the free-space impedance and that in the presence of a dielectric half-space for frequencies above 100 MHz. We have shown that a simple, series, *LC* resonant circuit can be used to exploit this difference to infer changes in SM. This can be accomplished by varying the capacitance to compensate for the inductive load presented by the loop antenna, which leads to a resonance condition and a current maximum. Equation 34 describes the relation between the resonant capacitance and the antenna's inductive reactance given by $\mathrm{Im}[Z(f_0)]$, where the impedance Z for a small circular loop antenna is theoretically evaluated as a function of antenna circuit and soil parameters in Sections 2–4. In particular, we show in Figure 4 that for a signal frequency $f_0 = 115$ MHz, and an antenna radius of 0.5 m, wire radius of 3 cm, and antenna height of 1 m, the antenna reactance $\mathrm{Im}[Z(f_0)]$ varies approximately from 20 to 60 Ω and the resonant capacitance C from 60 to 20 pF for volumetric soil moisture values spanning 0–0.4 g/cm^3. This range of sensitivities suggests that under ideal conditions bulk soil moisture can be retrieved with an accuracy on the order of 1% over horizontal scales spanning a few tens of meters to a few kilometers. Future work will focus on a proof-of-concept experimental verification of our results.

Data Availability Statement

This paper is a theoretical presentation. Data were not used nor created for this research.

Acknowledgments
The authors would like to thank the several reviewers whose comments significantly improved the clarity of the presentation. Alexander Voronovich was funded by the Physical Sciences Laboratory of the U.S. Department of Commerce National Oceanic and Atmospheric Administration. Paul Johnston was supported by the University of Colorado Cooperative Institute for Earth System Research and Data Science under Grant NA22OAR4320151. Richard Lataits was supported by the Science and Technology Corporation under contract number 1305M323FNRMJ0126.

References

Ashrafi, A., & Golnabi, H. (1999). A high precision method for measuring very small capacitance changes. *Review of Scientific Instruments*, *70*(8), 3483–3487. https://doi.org/10.1063/1.1149941

Babaeian, E., Sadeghi, M., Jones, S. B., Montzka, C., Vereecken, H., & Tuller, M. (2019). Ground, proximal, and satellite remote sensing of soil moisture. *Reviews of Geophysics*, *57*(2), 530–616. https://doi.org/10.1029/2018RG000618

Chang, D. (1973). Characteristics of a horizontal circular loop antenna over a multilayered, dissipative half-space. *IEEE Transactions on Antennas and Propagation*, *21*(6), 871–874. https://doi.org/10.1109/TAP.1973.1140599

Hardie, M. (2020). Review of novel and emerging proximal soil moisture sensors for use in agriculture. *Sensors*, *20*(23), 6934. https://doi.org/10.3390/s20236934

Jackson, J. D. (1999). *Classical electrodynamics*. John Wiley & Sons, Inc.

Kennedy, P. (1956). Loop antenna measurements. *IRE Transactions on Antennas and Propagation*, *4*(4), 610–618. https://doi.org/10.1109/TAP.1956.1144450

Li, Z.-L., Leng, P., Zhou, C., Chen, K.-S., Zhou, F.-C., & Shang, G.-F. (2021). Soil moisture retrieval from remote sensing measurements: Current knowledge and directions for the future. *Earth-Science Reviews*, *218*, 103637. https://doi.org/10.1016/j.earscirev.2021.103673

Mironov, V. L., Karavayskiy, A. Y., Lukin, Y. L., & Molostov, I. P. (2020). A dielectric model of thawed and frozen Arctic soils considering frequency, temperature, texture and dry density. *International Journal of Remote Sensing*, *41*(10), 3845–3865. https://doi.org/10.1080/01431161.2019.1708506

Moayyed, F., Oskouei, H. R. D., & Shirkolaei, M. M. (2021). High gain and wideband multi-stack multilayer anisotropic dielectric antenna. *Progress In Electromagnetics Research Letters*, *99*, 103–109. https://doi.org/10.2528/PIERL21062307

Mukhlisin, M., Astuti, H. W., Wardihani, E. D., & Matlan, S. J. (2021). Techniques for ground-based soil moisture measurement: A detailed overview. *Arabian Journal of Geosciences*, *14*(19), 2032. https://doi.org/10.1007/s12517-021-08263-0

Robock, A. (2003). *Encyclopedia of atmospheric sciences, HYDROLOGY | Soil Moisture* (pp. 987–993). Elsevier Science, LTD. https://doi.org/10.1016/B0-12-227090-8/00169-X

Ryu, J., Morrison, F., & Ward, S. H. (1970). Electromagnetic fields about a loop source of current. *Geophysics*, *35*(5), 862–896. https://doi.org/10.1190/1.1440134

Seneviratne, S. I., Corti, T., Davin, E. L., Hirschi, M., Jaeger, E. B., Lehner, I., et al. (2010). Investigating soil moisture–climate interactions in a changing climate: A review. *Earth-Science Reviews*, *99*(3–4), 125–161. https://doi.org/10.1016/j.earscirev.2010.02.004

Shirkolaei, M. M., & Aslinezhad, M. (2020). Substrate integrated waveguide filter based on the magnetized ferrite with tunable capability. *Microwave and Optical Technology Letters*, *63*(4), 1120–1125. https://doi.org/10.1002/mop.32722

Spears, J. H. (1989). *The relationship between ground permittivity and the input impedance of a horizontal dipole near the ground* (p. 74). US Army Corps of Engineers Construction Engineering Research Laboratory. Technical Manuscript M-89/05. https://apps.dtic.mil/sti/tr/pdf/ADA207746.pdf

Susha Lekshmi, S. U., Singh, D. N., & Baghini, M. S. (2014). A critical review of soil moisture measurement. *Measurement*, *54*, 92–105. https://doi.org/10.1016/j.measurement.2014.04.007

Voronovich, A. G., Johnston, P. E., & Lataitis, R. J. (2023). On equations for bent thin-wire Antennas. *IEEE Transactions on Antennas and Propagation*, *71*(2), 1234–1243. https://doi.org/10.1109/TAP.2022.3227803

Voronovich, A. G., & Lataitis, R. J. (2021). Soil moisture retrieval using reflection coefficients: Numerical experiments. *IEEE Transactions on Geoscience and Remote Sensing*, *59*(11), 8957–8967. https://doi.org/10.1109/TGRS.2020.3037012

Voronovich, A. G., & Lataitis, R. J. (2022). Soil moisture profile retrievals using reflection of multifrequency electromagnetic signals. *IEEE Transactions on Geoscience and Remote Sensing*, *60*, 1–10. https://doi.org/10.1109/TGRS.2022.3204522

Wait, J. R., & Spies, K. P. (1972). Subsurface electromagnetic fields of a circular loop of current located above ground. *IEEE Transactions on Antennas and Propagation*, *20*(4), 520–522. https://doi.org/10.1109/TAP.1972.1140232